Available online at www.sciencedirect.com
ScienceDirect
Journal of Catalysis 247 (2007) 145–154
JOURNAL OF CATALYSIS
www.elsevier.com/locate/jcat

# Pd nanoparticles with highly defined structure on MgO as model catalysts: An FTIR study of the interaction with CO, $O_2$, and $H_2$ under ambient conditions

H. Borchert [a], B. Jürgens [a], V. Zielasek [a], G. Rupprechter [b], S. Giorgio [c], C.R. Henry [c], M. Bäumer [a,*]

[a] *University of Bremen, Institute of Applied and Physical Chemistry, 28359 Bremen, Germany*
[b] *Vienna University of Technology, Institute of Materials Chemistry, 1210 Vienna, Austria*
[c] *CRMCN-CNRS, Campus de Luminy, Case 913, 13288 Marseille Cédex 9, France* [1]

Received 15 September 2006; revised 26 January 2007; accepted 1 February 2007

Available online 6 March 2007

**Abstract**

Model catalytic studies under ambient conditions require materials with well-defined structures for the establishment of clear relationships between structural and catalytic properties. In the present work, such a system was prepared by controlled decomposition of organometallic Pd precursors on a MgO support. The resulting Pd nanoparticles of highly defined morphology were characterized by high-resolution transmission electron microscopy and investigated with respect to their interaction with CO, $O_2$, and $H_2$ by IR spectroscopy (DRIFTS). Temperature-dependent CO adsorption experiments revealed the available adsorption sites on the Pd particles and indicated CO disproportionation on the Pd particles. We report in particular on the interplay between metal and support in these processes, which was analyzed by a thorough comparison of Pd/MgO with the pure MgO support. Investigations of the interaction with CO and $H_2$ suggest that Pd facilitates the formation of formates on MgO via dissociation of hydrogen on the Pd particles. Furthermore, CO oxidation was studied as a function of the $CO/O_2$ ratio in the temperature range 100–150 °C.


*Keywords:* Palladium; Magnesium oxide; Carbon monoxide; IR spectroscopy; Transmission electron microscopy

## 1. Introduction

Supported palladium particles have a wide range of applications as catalysts for technological processes, such as hydrogenation [1,2] and dehydrogenation reactions [3], methanation [4], CO oxidation [5,6] and NO reduction [7,8], and considerable efforts have been undertaken to gain more insight into the reaction mechanisms. In some cases, detailed information on relationships between structural and catalytic properties could be obtained in model catalytic studies under ultra-high-vacuum (UHV) conditions, in which single-crystal based samples with well-defined structures were exposed to small doses of gas molecules in a highly controlled manner [9–16]. However, the extent to which results obtained on model catalysts under UHV conditions remain meaningful for real catalysts under reaction conditions remains unclear [17–19]. For example, investigations of CO adsorption on Pd surfaces revealed that CO did not dissociate on Pd single-crystal surfaces [9], even when the surfaces were roughened by an Ar-sputtering technique and when the experiments were carried out at mbar pressures [20–22]. On real Pd catalysts, however, evidence of CO dissociation was found in some cases [9,20,23,24]. Particle size effects and metal–support interactions have been proposed to affect the ability of Pd catalysts to dissociate CO [9,21,23,24], but this topic remains under debate.

Elucidating clear relationships between structural and catalytic properties is much more complicated for real catalysts than in UHV studies, due to the usually more complex and less defined structure of real catalysts and the complexity of real reaction conditions. These difficulties promoted the preparation

* Corresponding author.
*E-mail address:* mbaeumer@uni-bremen.de (M. Bäumer).
[1] The CRMCN is associated to the Universities of Aix-Marseille II and III.

0021-9517/$ – see front matter 
doi:10.1016/j.jcat.2007.02.002

of model catalysts by wet-chemical methods with well-defined structural properties and their investigation under ambient conditions; for example, Lear et al. recently studied CO adsorption on alumina-supported Pd particles prepared from different palladium precursors [25,26]. Different surface structures obtained from the various preparations were correlated with frequency shifts and intensity changes in the IR spectra [25,26]. Bertarione et al. investigated the adsorption of CO [27] and methanol [28] on alumina- and magnesia-supported Pd particles by IR spectroscopy and found that the adsorption behavior of CO depended on the support material as well as the nature of the Pd precursor. When using Pd/MgO prepared from a $[Pd(NH_3)_4](NO_3)_2$ precursor, IR bands due to carbonates and bicarbonates on the support were observed in addition to bands corresponding to CO adsorption on Pd [27]; however, when using alumina as support or preparing Pd/MgO from a palladium chloride precursor, bands corresponding to carbonates and bicarbonates were absent [27]. Moreover, a detailed IR spectroscopic study of methanol adsorption allowed the authors to propose a mechanism of methanol decomposition, based on the observation of adsorbed CO forming on Pd after methanol exposure and annealing to ∼520 K [28].

Thorough investigations of chemically prepared Pd model catalysts remain rare; detailed studies of such systems are needed. Based on the controlled decomposition of organometallic precursors on magnesium oxide, we were able to prepare Pd nanoparticles on MgO that have well-defined properties with respect to crystallite size and morphology. In the present work, we present a systematic investigation of the interaction of CO, $O_2$, and $H_2$ with this well-defined Pd/MgO system and consider in particular the metal–support interplay. For this purpose, we combined high-resolution TEM measurements with IR spectroscopic investigations by DRIFTS (diffuse reflection infrared Fourier transform spectroscopy).

## 2. Experimental

Palladium nanoparticles on magnesium oxide were prepared by wet impregnation of MgO cubes (Fluka, specific surface 30 $m^2/g$) with palladium acetylacetonate [$Pd(acac)_2$] dissolved in acetonitrile. The solution was stirred, the solvent was evaporated, and the sample was dried at 80 °C for 3 h. Then the impregnated MgO powder was annealed in vacuum to 400 °C and reduced at the same temperature in $H_2$ at 400 mbar for 3 h. Using this technique, particles of different size and with different number densities were prepared depending on the precursor concentration [29]. For particle sizes <8 nm, the number density is equal to $\sim 10^3$–$10^4$ clusters/$\mu m^2$ and the size distribution is narrow. Previous work demonstrated that particles >10 nm obtained by the same technique are less well defined with respect to size and morphology [29]. In the present case, the preparation was conducted so as to obtain ∼6-nm particles.

TEM investigations were performed with a Jeol 3010 transmission electron microscope operated at 300 kV. IR spectroscopic experiments were performed in diffuse reflection geometry (DRIFTS) with a Biorad FTIR spectrometer (FTS 60A). Samples were pressed into pellets and studied in a reaction cell equipped with a controlled gas supply system, heating unit, and photometric detector (Hartmann & Braun URAS 10E) for CO and $CO_2$ gas analysis at the exit side of the cell. Before measurements, the samples were pretreated in the reaction cell under continuous gas flow of ∼50 $\%_{vol}$ $H_2$ in Ar for 1 h at 400 °C, then cooled under continuous Ar flow to the required temperature. Spectra were recorded with a resolution of $\leqslant 8$ $cm^{-1}$. All spectra shown are referenced to background spectra recorded under continuous Ar or $N_2$ flow after pretreatment.

## 3. Results and discussion

### 3.1. Structural characterization by transmission electron microscopy

Structural characterization of the samples was done by TEM. Fig. 1a shows an overview TEM image of the Pd/MgO sample, clearly showing individual Pd nanoparticles on cubic MgO support particles. The average diameter of the Pd nanoparticles is about 6 nm, as indicated by the size histogram in Fig. 1b. High-resolution images (Figs. 2a and 2b) show the particles growing

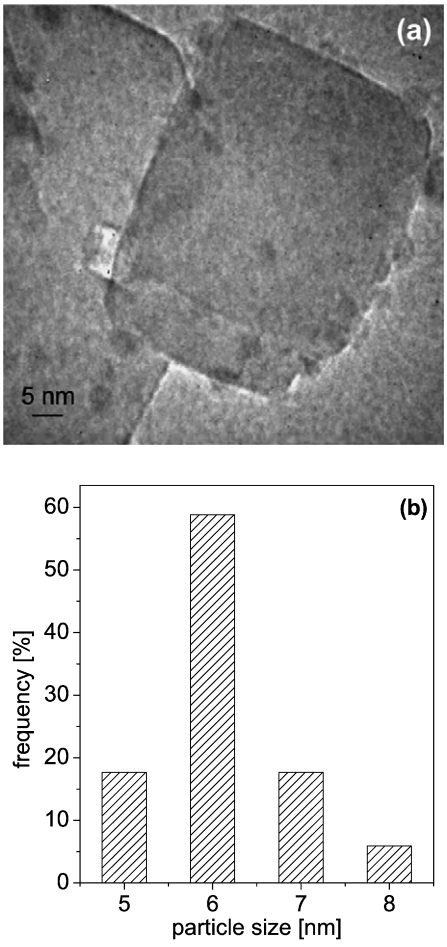


Fig. 1. (a) Overview TEM image of the Pd nanoparticles on MgO. (b) Histogram of the particle size distribution.

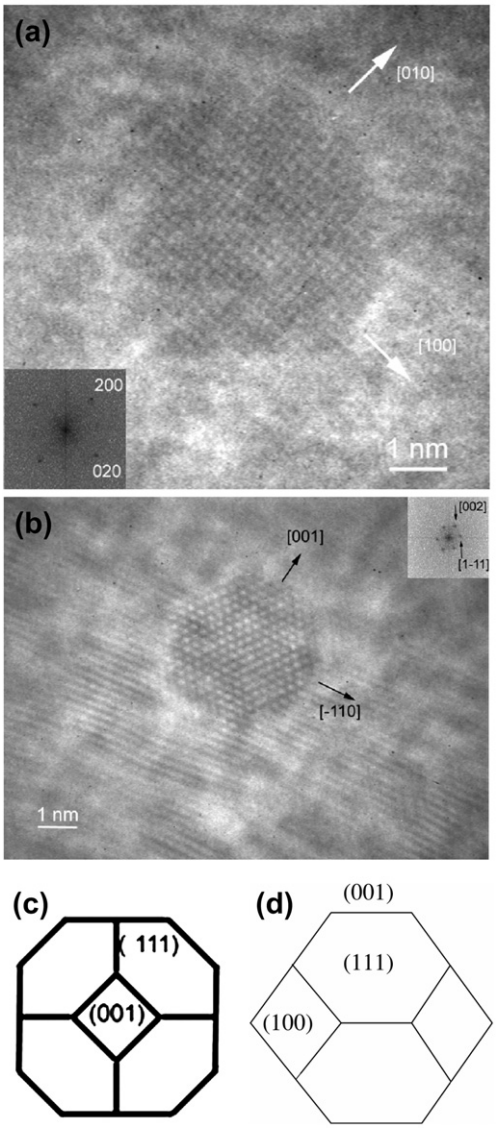


Fig. 2. (a) High-resolution TEM image of an individual Pd nanoparticle on MgO. The particle is oriented [001] in the electron beam. The particles posses a well-defined shape, limited by (001) and (111) faces which is illustrated by the schematic drawing in part (c) of the figure. (b) High-resolution TEM image of a Pd nanoparticle on MgO. The particle and the substrate are seen along the [110] direction. The accommodation with the substrate is clearly seen at the edges. The schematic drawing of the projection is shown in (d). (c) Schematic drawing of a truncated octahedron projected along a [001] direction. (d) Schematic drawing of a truncated octahedron projected along a [110] direction.

in defined epitaxial relations on the support; the (001) face of the Pd particles lies parallel to the (001) face of the MgO support, with the [100] axes of the Pd parallel to the [100] axes of the MgO lattice. Furthermore, the Pd nanoparticles have well-defined facets. The shape can be described as an octahedron with (111) facets with the corners truncated by (100) facets (cf. Figs. 2c and 2d). The high-resolution images and their power spectrum show perfect accommodation between the metal and oxide lattices. Thus, the Pd nanoparticles prepared on MgO in this work exhibit numerous well-defined structural features, making this system suitable for model catalytic studies under ambient conditions.

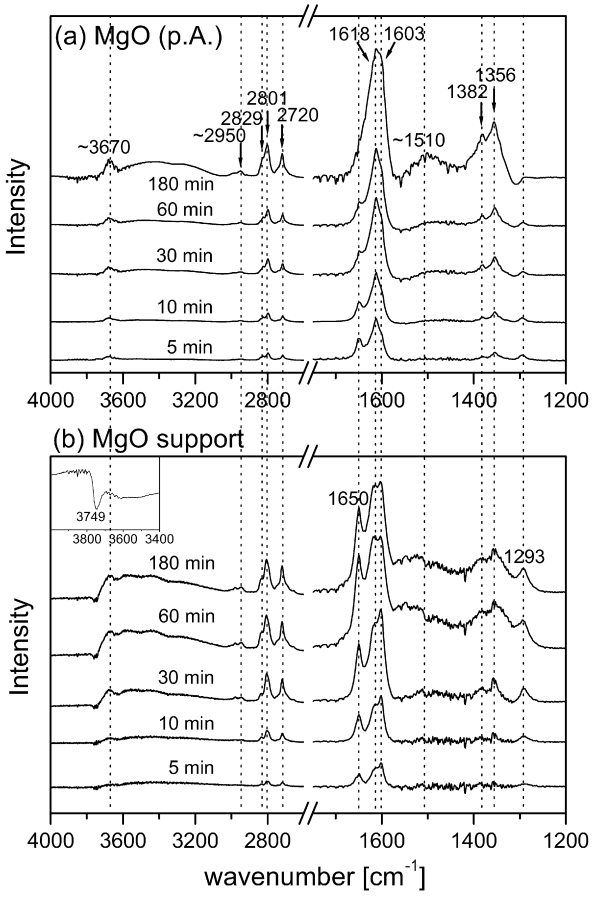


Fig. 3. IR spectra of (a) a reference MgO sample (Acros Organics, 16 $m^2/g$) and (b) the MgO used as support in this work (Fluka, 30 $m^2/g$) after exposure to a continuous gas flow of 0.1 $\%_{vol}$ CO in $N_2$ at 150 °C as a function of exposure time. The inset in (b) shows the O–H stretching region of the background spectrum recorded before CO exposure.

### 3.2. CO–MgO interaction

As a first step of the investigation of magnesia-supported Pd nanoparticles, we studied the interaction of CO with pure MgO. Apart from the MgO used as a support in the present work, an additional reference compound (Acros Organics, p.a. quality, 16 $m^2/g$) was also studied. Fig. 3 shows IR spectra for the two MgO samples. Spectra were recorded in a continuous gas flow of ∼0.1 $\%_{vol}$ CO in $N_2$ (total pressure: 1 bar) at 150 °C at exposure times of up to 3 h. In both cases, absorption bands developed in the O–H stretching region, the C–H stretching region, and the region below 1700 $cm^{-1}$, that is, well below the carbonyl-stretching region. The absence of bands in the carbonyl-stretching region is in agreement with studies of CO adsorption on MgO(001) revealing that molecular CO has a very low enthalpy of adsorption on MgO and can be seen only below ∼100 K under UHV conditions [30]. The continuous development of bands in the O–H and C–H stretching regions implies that there must be a source of hydrogen. Although the residual water content of the gases used was on the order of only a few ppm, this is apparently sufficient to supply water to the samples on the time scale of 3 h (details discussed below).

Table 1
Assignment of IR bands observed after CO adsorption on MgO at 150 °C

| IR band, wavenumber [$cm^{-1}$], this work | Literature | Assignment (lit.) | References |
|---|---|---|---|
| 1215 | 1220–1270 | Bidentate carbonate, bonded to 2 metal sites | [34] |
| 1293 | 1275, 1307 | Bidentate carbonate | [37] |
| | 1273, 1329 | Bidentate carbonate | [38] |
| | 1220–1270 | Bidentate carbonate, bonded to 2 metal sites | [34] |
| | 1250–1270 | Bidentate carbonate, bonded to 1 metal site | [34] |
| 1356, 1382 | 1348, 1385, 1390 | Formate | [32] |
| | 1340, 1390 | Formate | [34] |
| | 1360 | Formate | [33] |
| | 1370 | Formate | [31] |
| | 1370 | Monodentate carbonate | [37] |
| | 1300–1370 | Monodentate carbonate | [34] |
| ~1510 | 1472 | Carbonite | [31] |
| | 1535 | Monodentate carbonate | [37] |
| | 1470–1530 | Monodentate carbonate | [34] |
| 1603, 1618 | 1605 | Formate | [31] |
| | 1598 | Formate | [32] |
| | 1599 | Formate | [33] |
| | 1585, 1620 | Formate | [34] |
| 1650 | 1670 | Bidentate carbonate | [37] |
| | 1626, 1659 | Bidentate carbonate | [38] |
| | 1620–1670 | Bidentate carbonate, bonded to 2 metal sites | [34] |
| | 1530–1620 | Bidentate carbonate, bonded to 1 metal site | [34] |
| 2720, 2801, 2829, 2950 | 2728, 2820, 2931 | Formate | [32] |
| | 2820 | Formate | [31] |
| | 2730, 2830, 2957 | Formate | [33] |
| | 2760, 2840 | Formate | [34] |
| ~3400 | | $H_2O$, multiple bonded | |
| 3670 | | $Mg(OH)_2$ | |

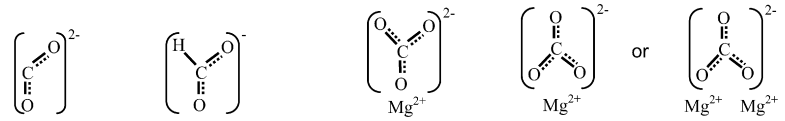


The frequencies of the bands, as well as their assignments, are summarized in Table 1. Both magnesia samples showed bands at ~1356, ~1382, ~1603, ~1618, ~2720, ~2801, ~2829, and ~2950 $cm^{-1}$. All of these bands can clearly be assigned to formate species [31–34]. The splitting of the band at around ~1600 $cm^{-1}$ indicates the presence of two slightly different types of formate species, probably due to the existence of two types of hydroxyl groups on MgO, as discussed by Davidov [34]. After exposure of more than 1 h, an additional broad band appeared at around ~1510 $cm^{-1}$ that could be due to carbonite ions ($CO_2^{2-}$) resulting from the interaction of CO with coordinatively unsaturated $O^{2-}$ ions at the MgO surface [31,35,36], or to monodentate carbonate species [35,37]. The band at ~3670 $cm^{-1}$ and the broad band at ~3400 $cm^{-1}$ are probably due to $Mg(OH)_2$ configurations and adsorbed water molecules, respectively. Note that isolated hydroxyl groups on MgO were reported to give rise to a rather sharp band at around 3750 $cm^{-1}$ [33,34]. Such bands were visible in the background spectra recorded before exposure to CO (Fig. 3b, inset), but additional isolated hydroxyl groups do not seem to develop on exposure to CO, as indicated by the absence of a band at 3750 $cm^{-1}$ in the spectra referenced to the background (see Fig. 3).

In addition to the bands discussed so far, two resonances at 1650 and ~1293 $cm^{-1}$ were more pronounced in the MgO sample used as the support material in this work. These bands indicate the formation of bidentate carbonate species, presumably bonded to two $Mg^{2+}$ cations [34,37,38]. The formation of carbonate species probably is related to residual oxygen in the system. Smart et al. studied CO adsorption on MgO at different pressures and observed carbonate formation even at $1.3 \times 10^{-5}$ mbar [37]. With increased exposure time, the relative intensity of the bands corresponding to bidentate carbonates decreased, and mainly bands corresponding to formates developed at the considered temperature of 150 °C.

Another noteworthy temporal evolution in the IR spectra was seen. In the first ~30 min, formate species rapidly appeared in the spectra. Afterwards, the band possibly corresponding to carbonite ions began to develop while the formate formation slowed. In a study of CO adsorption on CaO and MgO, Babaeva et al. found that the development of formates on CaO proceeded at 300 K via the formation of carbonite ions as an intermediate species [31]. Carbonite ions have been found to react to formates in the presence of water vapor [31]. The authors found many similarities between CaO and MgO and observed the for-

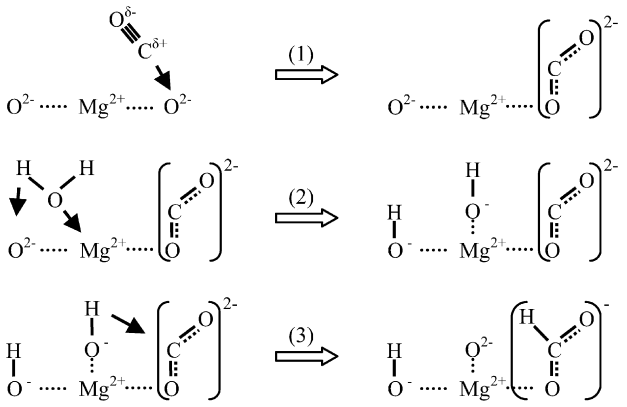

Fig. 4. Possible, schematic mechanism of formate formation on MgO at 150 °C.

mation of carbonite ions also on MgO [31]. Based on these investigations, a reaction mechanism can be suggested to explain the temporal behavior observed in the present study (see Fig. 4). In a first step, CO adsorbs on a coordinatively unsaturated $O^{2-}$ site on the MgO surface and forms a carbonite ion. Next, a water molecule adsorbs on MgO and dissociates, resulting in the formation of two OH groups at the surface [39]. In a third step, the carbonite ion then reacts with a neighboring OH group to formate. In principle, step 3 may occur with the OH groups generated during the experiment by residual water in the gas feed, as well as with the OH groups already present on the MgO surface after $H_2$ pretreatment at 400 °C. If the carbonite ions were highly reactive with respect to neighboring OH groups, this would explain why the (rapid) formation of formates is observed only initially. At a later stage of the experiment, suitable sites with carbonite ions having an OH group in their vicinity would become increasingly rare, thereby slowing this reaction pathway and leading to a build-up of carbonite ions.

Finally, we should mention that the reactive adsorption of CO on MgO is also temperature-dependent. At 30 °C, formates were not generated under these conditions (data not shown). Exposure to a continuous gas flow of CO in Ar for several minutes led to IR bands at ∼1300, ∼1380, ∼1530, and ∼1650 $cm^{-1}$, indicating the formation of mono- and bidentate carbonate species [37,38]. Davidov also reported that temperatures above 100 °C are required for formate production on MgO [34].

### 3.3. Interaction of CO and Pd/MgO: CO adsorption sites

The adsorption of CO on Pd nanoparticles on MgO was studied at 30 °C by exposing samples to a continuous gas flow of ∼0.1 $\%_{vol}$ CO in Ar for 10 min. A corresponding IR spectrum is shown in Fig. 5 (bottom spectrum). Three absorption bands are visible at ∼1904, ∼1983, and ∼2063 $cm^{-1}$ that can be assigned, from low to high wavenumbers, to CO on threefold-hollow sites of Pd(111) facets, to bridge-bonded CO on various Pd sites, and to CO linearly bonded to Pd atoms, respectively [18,19,25–27,40–43].

In particular, the band corresponding to linearly bonded CO merits discussion. In a study of Pd particles supported

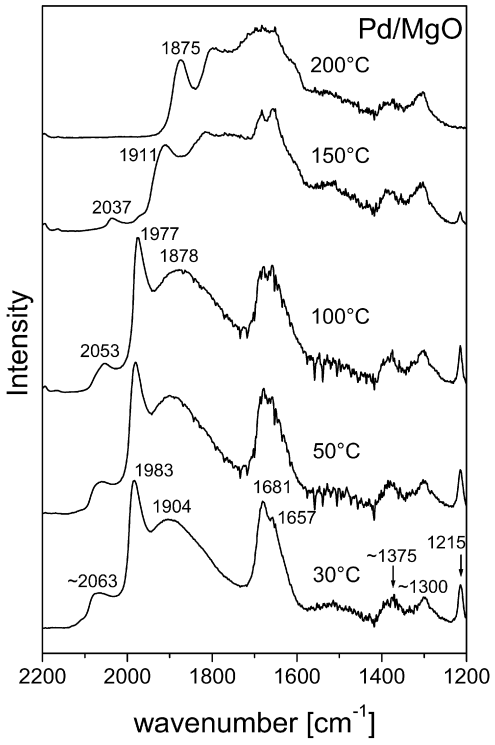


Fig. 5. IR spectra of Pd nanoparticles on MgO after exposure to CO. Initially, the sample was exposed to a continuous gas flow of 0.1 $\%_{vol}$ CO in Ar for 10 min at room temperature (bottom spectrum). The sample was then heated under pure Ar gas flow, kept for 10 min at the indicated temperature and cooled down again to *RT* before the next spectrum was measured.

on $Al_2O_3$ and MgO, Bertarione et al. assigned bands at ∼2025–2076 $cm^{-1}$ to CO linearly bonded to Pd atoms on edges, steps, and terraces of (100) and (111) facets [27]. A more detailed assignment based on UHV studies of CO adsorption on Pd particles grown on a thin alumina film also has been reported [18,19,41–43]. Pd particles of various sizes and morphologies could be prepared on this support, depending on the growth temperature. At 300 K, large (7–10 nm), well-ordered Pd crystallites exposing mainly (111) facets were obtained, whereas at 90 K, small (mean size ∼2 nm), disordered Pd particles resulted from physical vapor deposition. For the well-faceted particles, a sharp band at ∼2100 $cm^{-1}$ was observed at saturation coverage and 90 K and was ascribed to terminally bonded CO on (111) terraces. For the small, disordered particles, however, adsorption at 90 K led to a rather broad band at 2050–2130 $cm^{-1}$. This was attributed to terminal CO adsorption on edge and corner atoms, because well-developed facets were basically absent on the small particles.

Apart from surface roughness, the population of linear sites (on-top CO) is also dependent on temperature and CO pressure. Dellwig et al. studied the CO pressure dependence systematically at 200 K using sum-frequency generation spectroscopy [17]. Whereas at $10^{-7}$ mbar only bridge-bonded CO was observed for well-faceted 6-nm Pd particles, at higher pressures ($10^{-3}$–200 mbar), bands corresponding to linearly bonded CO on (111) surfaces also occurred [17]. Up to ∼1 mbar, those bands were comparably weak, but at 200 mbar they were even more intense than those corresponding to bridge-

bonded CO [17]. A similar pressure/coverage dependence was also reported for Pd(111) single-crystal surfaces [22,44,45]. In contrast, for the disordered particles, the band centered at 2100 $cm^{-1}$ was observed over the whole pressure regime [17].

Lear et al. took a further step and investigated the morphology-dependent occupation of different sites on alumina-supported Pd particles prepared from various precursors [25]. In the case of tetraaminepalladium(II) tetraazidopalladate(II) [Pd(azide)], Pd particles with an average diameter of about ∼15 nm and a well-defined crystallite morphology were obtained [26]. The crystallites exposed mainly (111) and (100) planes and were assumed to be rather defect-free [25,26]. In this case, the IR bands of terminally bonded CO were extremely weak [25]. Because the experiments were done by pulsing CO onto the sample, not by applying a static CO pressure, it was concluded that CO does not populate linear sites on the terraces at low partial pressure, in agreement with the findings of Dellwig et al. [17]. In addition, the absence of surface roughness limits the occurrence of on-top CO.

Using $Pd(acac)_2$ as precursor (i.e., the same precursor as in the present study), Lear et al. obtained particles much smaller than those obtained from the Pd(azide) precursor and those used in the present study [25]. These particles could not be analyzed in detail by TEM. For these catalysts, an intense and sharp band was observed at ∼2080 $cm^{-1}$ that disappeared on heating the sample to about 150 °C. Because of the small size of the particles (∼1.5 nm, determined indirectly from chemisorption measurements), the authors assigned this peak to CO terminally bonded to corner atoms [25].

In contrast, other precursors also yielding small disordered Pd particles typically resulted in two IR bands with different desorption behaviors [25]. Bands in the range of ∼2077–2090 $cm^{-1}$, disappearing at 150 °C, were assigned to CO terminally bonded to corner atoms, in analogy to the $Pd(acac)_2$ system [25]. The other band, detected in the range of ∼2050–2064 $cm^{-1}$ and exhibiting a much higher desorption temperature of ∼300 °C, was assigned to on top CO on Pd atoms at (111)/(111) and (111)/(100) edges [25].

However, according to theoretical calculations, the chemisorption energy of CO linearly bonded to different Pd sites is expected to increase with decreasing coordination of the adsorption site [9,46]. Thus, CO bonded to Pd edge atoms would be expected to desorb at lower temperature than CO bonded to corner atoms, which is in disagreement with the assignment proposed by Lear et al.

Our present results help clarify the situation. Because the CO partial pressure was around 1 mbar in our experiments, linear CO adsorption on Pd atoms of (111) surfaces presumably plays only a minor role, as reported by Dellwig et al. [17] and Lear et al. [25]. The high-resolution TEM images provide evidence that our palladium particles are well-shaped and have mainly (111) and (100) facets (cf. Fig. 2); therefore, considerable surface roughness that could induce CO bonding to on-top sites is absent. Due to the average particle size of ∼6 nm, a considerable fraction (15%) of Pd atoms is located at the (111)/(111) and (111)/(100) edges. (For a general discussion of the number of various surface sites as a function of crystallite size and shape, see [47].) Therefore, it is reasonable to assign the on-top species observed in the present study to CO linearly bonded to Pd edge atoms. Note that we cannot fully exclude on-top adsorption on (111) facets, but these species typically have higher frequencies [44], and are more likely to be responsible for the very small shoulder which is discernible around ∼2100 $cm^{-1}$ in the IR spectra after CO adsorption at room temperature (bottom spectrum in Fig. 5).

To determine the desorption temperature of the on-top species, we performed annealing experiments. After initial CO adsorption at room temperature (bottom spectrum in Fig. 5), the sample was heated under pure Ar gas flow, kept for 10 min at the respective temperature, and then cooled to room temperature for IR spectroscopy (the other spectra shown in Fig. 5). The band assigned to CO linearly bonded to Pd edge atoms nearly fully disappeared after annealing to ∼150 °C, whereas the other bands remained present. In analogy to the findings of Lear et al., the annealing experiments led to shifts of all adsorption bands of CO on Pd sites to lower wavenumbers, with a more pronounced effect for the bridge-bonded and threefold-bonded CO species than for the linearly bonded species. These shifts can be explained by reduced dipole coupling at decreased CO coverage. The desorption temperature of the band clearly assigned to CO on Pd edges in our work is very similar to the desorption temperature of the band observed at ∼2077–2090 $cm^{-1}$ by Lear et al. Therefore, we propose that the peak at higher frequency in the study of Lear et al. is also caused by edge atoms, whereas the second band at lower frequency arises from defect sites with even lower coordination. This assignment is also in agreement with the lower frequency of the latter species, because the lower-coordinated Pd atoms are expected to have a higher capability for electron back donation to the CO $2\pi^*$ orbitals, resulting in more red-shifted stretching frequencies [9].

### 3.4. Interaction of CO and Pd/MgO: Reaction

In addition to the bands discussed in the previous section, the spectra of the Pd/MgO system also contain bands in the region below 1700 $cm^{-1}$, which indicate reactive adsorption of CO on MgO, as in the case of the pure MgO support. At room temperature, bands were observed at ∼1300, ∼1375, ∼1500, and 1657 $cm^{-1}$ (see Fig. 5). As discussed in Section 3.2, bands at ∼1300 and 1657 $cm^{-1}$ can be assigned to bidentate carbonate species [34,37,38]. The bands at ∼1375 and ∼1500 $cm^{-1}$, on the other hand, indicate monodentate carbonate species [34]. Bands indicative of formate formation were not observed on CO adsorption on the supported Pd particles at room temperature, in agreement with the absence of formates on pure MgO below 100 °C (see Section 3.2).

In addition to the bands discussed so far, a prominent peak at 1681 $cm^{-1}$ was discernible in the spectra, accompanied by a band at 1215 $cm^{-1}$. These bands are definitely absent for the unloaded MgO support and can be attributed to carbonate [32], probably to a bidentate species bonded to two metal sites [34,37].

Insight into the origin of this species is obtained by considering the temperature-dependent experiments shown in Fig. 6.

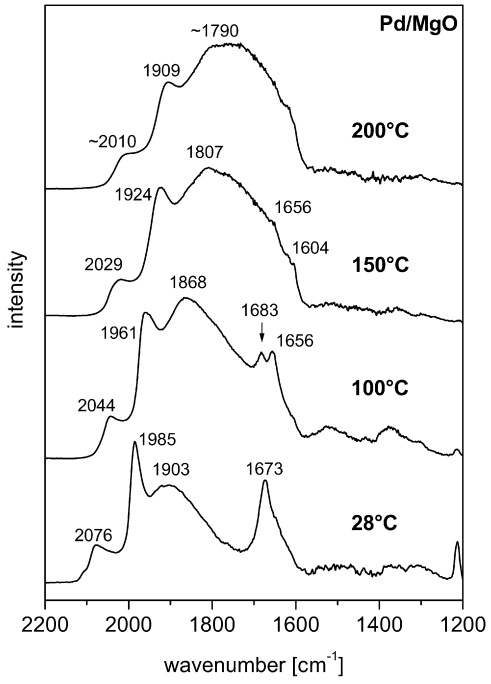


Fig. 6. IR spectra of Pd nanoparticles on MgO after exposure to a continuous gas flow of 0.1 $\%_{vol}$ CO in Ar at different temperatures. All spectra were recorded after 5 min of exposure.

The IR spectra were recorded at room temperature and 100, 150, and 200 °C for Pd/MgO under a continuous gas flow of 0.1 $\%_{vol}$ CO in Ar, each after 5 min of exposure. With increasing temperature, the bands corresponding to CO adsorption on Pd shift to lower wavenumbers. Furthermore, the relative intensities of the bands corresponding to the different adsorption sites of CO on Pd change in favor of the threefold-hollow sites, in agreement with the order of the enthalpy of adsorption. Along with the temperature-dependent adsorption of CO on different Pd sites, a clear temperature dependence of the peaks at 1681 and 1215 $cm^{-1}$ is evident. These carbonate bands are much more pronounced at room temperature than at elevated temperatures.

This finding clearly indicates that Pd gives rise to a temperature-dependent formation of a new carbonate species on the MgO support on exposure to CO. A possible explanation for this is the disproportionation of CO on Pd,

$$2CO \rightarrow CO_2 + C, \quad (1)$$

which can be considered the net reaction of CO dissociation and subsequent reaction of the oxygen atom with another CO molecule to $CO_2$ [20]. Whereas $CO_2$ can react with coordinatively unsaturated $O^{2-}$ ions to carbonate species on MgO, the elemental C atoms probably remain on the Pd particles. Because the overall reaction is exothermic, these processes should become less pronounced at higher temperatures, as indeed was observed.

As mentioned in Section 1, CO dissociation (disproportionation) on Pd is a topic that remains under debate. There is agreement that CO does usually not dissociate on Pd single-crystal surfaces [9,20–22]. Only in the case of Pd(112) was CO dissociation on step sites observed [48]. For supported Pd catalysts under ambient conditions, some authors have reported CO dissociation, whereas others have not. Bertarione et al. conducted an IR spectroscopy study of Pd particles on MgO prepared from palladium chloride (particle size $\sim 15 \pm 3.5$ nm) and from $[Pd(NH_3)_4](NO_3)_2$ precursors (mean particle size $\sim 11 \pm 4.5$ nm) [27]. In the case of $[Pd(NH_3)_4](NO_3)_2$, they observed carbonate and bicarbonate species after CO adsorption at room temperature, and took the appearance of the corresponding IR bands as an indication of disproportionation of CO on Pd [27]. In the case of particles prepared from the chloride precursor, they found no indications for CO disproportionation, but could not determine whether this was due to the larger Pd particle size or to the surface basicity of MgO, which was reduced by the presence of $Cl^-$ ions [27]. Prinetto et al. studied CO adsorption at room temperature on dispersed Pd on MgO, $Al_2O_3$, and Mg(Al)O mixed oxides [24]. For highly dispersed systems (particle size <2 nm), the authors observed CO disproportionation only for MgO-supported Pd, demonstrating the role of metal–support interactions [24]. Furthermore, the dispersion was shown to be of importance. Prinetto et al. [24] did not observe CO disproportionation for larger Pd particles (~3–4 nm) on MgO. This is in contrast to Bertarione et al.'s observation of CO disproportionation on much larger Pd particles on MgO (see above).

Our work, which was also extended to higher temperatures, can shine some more light on the phenomenon of CO disproportionation on magnesia-supported Pd particles. As shown by the temperature-dependent measurements, disproportionation of CO and formation of carbonate species on MgO become less pronounced at higher temperature. At room temperature, large amounts of carbonate develop rapidly compared with pure MgO. At 200 °C, almost no carbonates are observed, in agreement with the shift of the equilibrium of the Boudouard reaction to the CO side. This observation shows that $CO_2$ resulting from the disproportionation reaction is bound reversibly on MgO, presumably in the neighborhood of the particles, because otherwise, intense carbonate bands would also be expected in the high-temperature regime. We note that at 200 °C, the formation of carbonates with subsequent decomposition can be excluded. Carbonate decomposition on MgO would require temperatures above ~400 °C [38,49].

Moreover, we want to mention that in some cases, prolonged CO exposure (~30 min) led to slight temporal changes in the spectra (not shown). A small increase of the carbonate band was accompanied by changes in the relative intensities of the bands corresponding to CO adsorption on the different Pd sites. In agreement with other investigations [50,51], these correlations would be compatible with a mechanism in which elemental carbon formed on CO disproportionation blocks threefold-hollow sites on the Pd surface. Nevertheless, further experiments are needed to support this interpretation.

Another noteworthy result of the temperature-dependent measurements concerns the formation of formate species. Although no indications for formates were found up to 100 °C, a small shoulder at ~1604 $cm^{-1}$ indicative of formates appeared in the spectrum at 150 °C (see Fig. 6). This finding

was confirmed by the appearance of small bands in the C–H stretching region that were not observed up to 100 °C. Formate is probably generated independently, as on pure MgO at 150 °C. However, compared with pure MgO, the bands corresponding to formates were weak in the case of the supported Pd particles and remained weak even after prolonged CO exposure (∼30 min). This shows that formate formation on MgO was largely suppressed by the presence of the Pd nanoparticles. A possible reason for this could be that Pd blocks sites favorable for the formation of formates or catalyzes their decomposition. Blocking phenomena were also observed for Cu deposited on ZnO [52].

### 3.5. Interaction of CO and $O_2$ with Pd/MgO

Next, we used the Pd/MgO system as a model catalyst for CO oxidation. Fig. 7 depicts an experiment in which the sample was exposed to a 1:1 vol% $CO/O_2$ mixture in the reaction cell of the IR spectrometer. The first spectrum (designated "a") was recorded at 150 °C on exposure to CO only and exhibited the characteristics discussed earlier. When oxygen was added to the gas feed, the bands corresponding to CO adsorption on Pd sites disappeared almost immediately (spectrum "b"). Furthermore, an immediate increase of the bands corresponding to carbonate species on the MgO support is visible. Fig. 7b shows the CO and $CO_2$ concentrations measured at the exit side of the gas cell. Obviously, CO is oxidized to $CO_2$ at 150 °C. We note that absolute conversion rates cannot be determined in this experiment, because the construction of the gas cell is not suitable for this purpose. (A considerable fraction of the feed gas can pass the cell without coming in contact with the catalyst.) Gaseous $CO_2$ is also visible in the IR spectra (the band at ∼2348 $cm^{-1}$.)

Whereas the Pd particles were definitely metallic after the hydrogen pretreatment and during CO adsorption (reducing conditions), the state of Pd during the CO oxidation experiments is not a priori clear. In general, the oxidation state can have an important influence on the activity and selectivity in oxidation reactions [53–55], and recent studies have shown that different phases of palladium oxide can form under oxidative reaction conditions [54–56]. In studies of Pd-based model catalysts prepared under UHV conditions, dissociative chemisorption of oxygen was found up to ∼450 K, whereas the formation of palladium oxide phases required temperatures above ∼500 K [56,57]. The activity for CO oxidation was found to decrease with increasing coverage of the Pd surface by oxides for such model systems [54,55].

Spectrum "c" in Fig. 7a, recorded directly after switching off $O_2$, exhibits only minor differences from the spectrum recorded before exposure to oxygen (spectrum "a"). The frequencies of the bands corresponding to CO adsorbed on Pd are shifted slightly to higher wavenumbers, and the intensity of the bands corresponding to linearly and bridge-bonded CO are increased slightly at the expense of the band corresponding to threefold-bonded CO. The integrated intensity of all three bands together decreased by ∼6%. These changes provide an indication that the surface might be partly oxygen-covered after exposure to the $CO/O_2$ atmosphere at 150 °C. But because the loss of intensity of the bands corresponding to CO on metallic Pd sites is only a few percent, and because bands corresponding to CO adsorbed on $Pd^{2+}$ cations remain absent, the degree of oxidation is small. Thus, the postreaction IR data show that the Pd model catalyst is almost entirely in the metallic state *after*

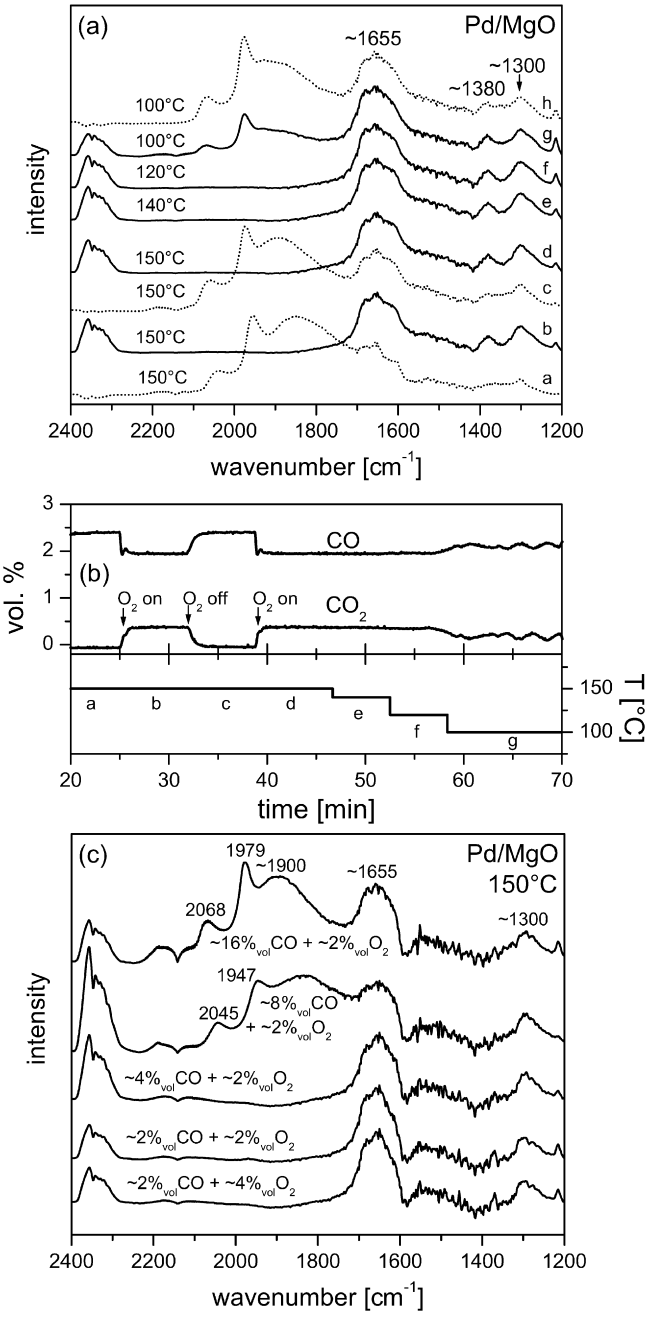


Fig. 7. (a) IR spectra of Pd nanoparticles on MgO after exposure to a continuous gas flow of $CO/O_2$ mixtures in Ar at different temperatures. Spectra plotted as solid lines correspond to exposure to ∼2 $\%_{vol}$ CO and ∼2 $\%_{vol}$ $O_2$. Spectra plotted as dotted lines correspond to exposure to CO only ($O_2$ switched off). (b) Plot of the CO and $CO_2$ concentration measured by the photometric detector as a function of time. The applied temperatures are also plotted, and the labels "a"–"g" indicate in which period the IR spectra in part (a) of the figure were measured. The spectrum "h" was measured at the end of the experiment, i.e., after switching off $O_2$. (c) IR spectra of Pd nanoparticles on MgO after exposure to a continuous gas flow of different $CO/O_2$ mixtures in Ar at 150 °C.

*exposure to CO/$O_2$* at 150 °C, which is in agreement with the findings that palladium oxide phases do not form on Pd model catalysts prepared under UHV conditions in this temperature regime [54–57]. Because the formation of oxide phases may also depend on pressure and structural properties, we cannot fully exclude the possibility that palladium oxide phases are reversibly formed in the $CO/O_2$ atmosphere *during reaction* at 150 °C in our case.

After switching $O_2$ on again, we lowered the temperature to find the lowest temperature at which CO oxidation can be observed for this system. Down to 120 °C we see no differences by either IR spectroscopy or analysis of the gas phase. At 100 °C, however, the conversion drops, as revealed by photometric detection. Simultaneously, the IR bands corresponding to CO adsorption on Pd reappear, but do not show the same intensity as in the absence of oxygen (compare spectra "g" and "h"). However, there do not seem to be large differences in the relative intensities of the bands corresponding to different adsorption sites compared with spectra recorded on exposure to CO only.

Experiments with different gas-phase compositions were also performed. Fig. 7c shows IR spectra recorded at 150 °C on exposure to $CO/O_2$ gas mixtures with compositions between 1:2 and 8:1. In the case of CO excess (ratio > 2:1), adsorbed CO species are observed during the ongoing CO oxidation reaction, whereas no adsorbed CO is detectable for lower ratios. This can be explained by the usually sharp transition from a oxygen-saturated system to a CO-saturated system typical for the CO oxidation reaction also showing kinetically two distinct reaction regimes (oxygen-rich and CO-rich) [58].

### 3.6. Interaction of CO and $H_2$ with MgO and Pd/MgO

Finally, we studied the Pd particles and pristine magnesia support with respect to their interaction with carbon monoxide and hydrogen. Vibrational studies of CO/H on Pd(111) and Pd particles on alumina under both UHV and ambient pressure conditions, which may serve as references were reported in [59,60]. Fig. 8a shows IR spectra for pure MgO exposed to CO and $H_2$ in Ar. As discussed in Section 3.2, in the absence of $H_2$ mainly formate species develop at 150 °C. At this temperature, the addition of hydrogen to the feed gas does not result in a significant increase of the corresponding IR bands. Thus, and not unexpectedly, molecular hydrogen obviously cannot act as a hydrogen source for formate formation on MgO at 150 °C. Raising the temperature to 250 °C leads to a slightly increased intensity of the IR bands and to some changes in the relative intensities of the bands in the C–H stretching region.

For Pd particles on MgO at 150 °C, addition of hydrogen to the feed gas had no pronounced effect (see Fig. 8b), in agreement with a study by Morkel et al. [60]. Spectra before and after addition of $H_2$ revealed only a small band around ~1605 $cm^{-1}$ indicative of formates, because disproportionation of CO and carbonate formation seem to be the predominant processes, as discussed before. Obviously, the hydrogen supply does not favor generation of formates at 150 °C. However, higher temperatures increase the intensity of the bands corresponding to

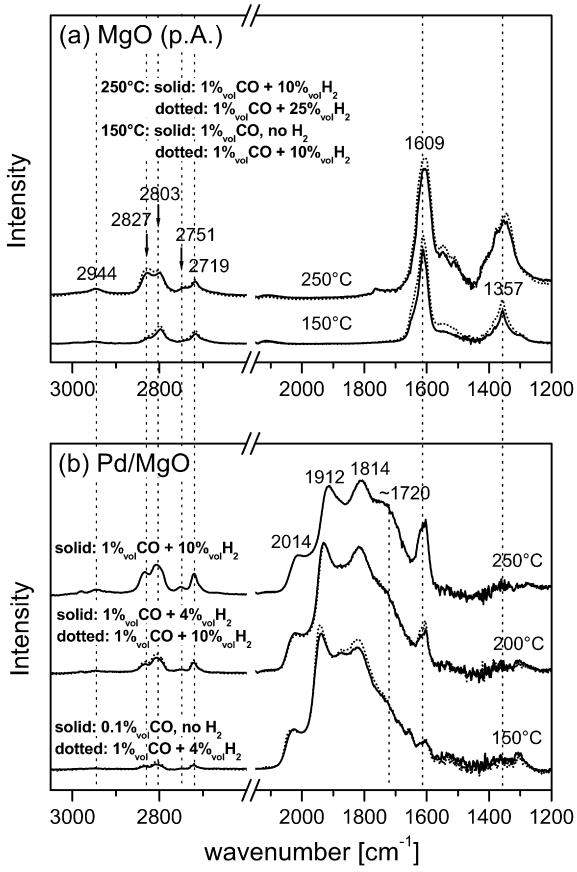


Fig. 8. IR spectra of (a) MgO and (b) Pd nanoparticles on MgO after exposure to a continuous gas flow of $CO/H_2$ mixtures in Ar at different temperatures. All spectra were recorded after relatively short exposure times of a few minutes.

formates compared with the situation without $H_2$ in the feed (cf. Fig. 6). This finding suggests that above ~200 °C, atomic hydrogen formed by dissociation on Pd can serve as a source of atomic hydrogen for formate generation on the MgO support. Because hydrogen is known to dissociate on Pd even at temperatures as low as 20 K, the rate-limiting step is probably a spillover process of atomic hydrogen from the Pd particles to the MgO support.

## 4. Conclusion

In the present work, we prepared Pd nanoparticles on MgO by controlled decomposition of organometallic precursors. High-resolution TEM measurements revealed that these particles have well-defined structural properties that make them suitable as a model system for fundamental catalytic studies under ambient conditions. We investigated their interaction with CO, $O_2$, and $H_2$ and performed IR spectroscopic experiments. In the regime of terminally bonded CO on the Pd particles, a peak at ~2060–2070 $cm^{-1}$ could be assigned to adsorption at crystallite edge sites. CO adsorption was accompanied by disproportionation of CO on the Pd particles. Whereas elemental carbon seems to remain on the Pd particles, possibly blocking threefold-hollow sites, $CO_2$ can react further with coordinatively unsaturated $O^{2-}$ ions of the MgO support to car-

bonate species. Systematic studies at temperatures up to 200 °C revealed that this phenomenon is less pronounced at higher temperature. Studies of the interaction with CO and $O_2$ showed that the model catalysts were active for CO oxidation at temperatures above ∼100 °C, and investigations of the interaction with CO and $H_2$ suggested that Pd facilitated the formation of formates on MgO at temperatures above ∼200 °C via dissociation of hydrogen on the Pd particles.

## Acknowledgments

The authors thank U. Melville and K. Koblitz for technical assistance with the IR spectroscopic measurements and Y. Borchert for useful discussions. This work was supported by the German Science Foundation within the framework of SPP 1091.

## References

[1] R.L. Burwell Jr., Langmuir 2 (1986) 2.
[2] A. Borodzinski, A. Golebiowski, Langmuir 13 (1997) 883.
[3] P.D. Tien, T. Satoh, M. Miura, M. Nomura, Energy Fuels 19 (2005) 731.
[4] M.A. Vannice, R.L. Garten, Ind. Eng. Chem. Prod. Res. Dev. 18 (1979) 186.
[5] S.-H. Oh, G.B. Hoflund, J. Phys. Chem. A 110 (2006) 7609.
[6] A.M. Venezia, L.F. Liotta, G. Pantaleo, V. La Parola, G. Deganello, A. Beck, Z. Koppany, K. Frey, D. Horvath, L. Guczi, Appl. Catal. A 251 (2003) 359.
[7] H.G. Stenger Jr., J.S. Hepburn, Energy Fuels 1 (1987) 412.
[8] J.S. Hepburn, H.G. Stenger Jr., Energy Fuels 2 (1988) 289.
[9] C.R. Henry, Surf. Sci. Rep. 31 (1998) 231.
[10] M. Frank, M. Bäumer, Phys. Chem. Chem. Phys. 2 (2000) 3723.
[11] H.-J. Freund, M. Bäumer, H. Kuhlenbeck, Adv. Catal. 45 (2000) 412.
[12] T.P.St. Clair, D.W. Goodman, Top. Catal. 13 (2000) 5.
[13] K.H. Hansen, Z. Sljivancanin, E. Lægsgaard, F. Besenbacher, I. Stensgaard, Surf. Sci. 505 (2002) 25.
[14] D.W. Goodman, J. Catal. 216 (2003) 213.
[15] H.-J. Freund, M. Bäumer, J. Libuda, T. Risse, G. Rupprechter, S. Shaikhutdinov, J. Catal. 216 (2003) 223.
[16] S.L. Tait, Z. Dohnalek, C.T. Campbell, B.D. Kay, Surf. Sci. 591 (2005) 90.
[17] T. Dellwig, J. Hartmann, J. Libuda, I. Meusel, G. Rupprechter, H. Unterhalt, H.-J. Freund, J. Mol. Catal. A 162 (2000) 51.
[18] T. Dellwig, G. Rupprechter, H. Unterhalt, H.-J. Freund, Phys. Rev. Lett. 85 (2000) 776.
[19] H. Unterhalt, G. Rupprechter, H.-J. Freund, J. Phys. Chem. B 106 (2002) 356.
[20] G. Rupprechter, V.V. Kaichev, H. Unterhalt, M. Morkel, V.I. Bukhtiyarov, Appl. Surf. Sci. 235 (2004) 26.
[21] V.V. Kaichev, M. Morkel, H. Unterhalt, I.P. Prosvirin, V.I. Bukhtiyarov, G. Rupprechter, H.J. Freund, Surf. Sci. 566–568 (2004) 1024.
[22] V.V. Kaichev, I.P. Prosvirin, V.I. Bukhtiyarov, H. Unterhalt, G. Rupprechter, H.-J. Freund, J. Phys. Chem. B 107 (2003) 3522.
[23] V. Matolin, E. Gillet, Surf. Sci. 238 (1990) 75.
[24] F. Prinetto, M. Manzoli, G. Ghiotti, M. de Jesus Martinez Ortiz, D. Tichit, B. Coq, J. Catal. 222 (2004) 238.
[25] T. Lear, R. Marshall, J.A. Lopez-Sanchez, S.D. Jackson, T.M. Klapötke, M. Bäumer, G. Rupprechter, H.-J. Freund, D. Lennon, J. Chem. Phys. 123 (2005) 174706.
[26] T. Lear, R. Marshall, E.K. Gibson, T. Schütt, T.M. Klapötke, G. Rupprechter, H.-J. Freund, J.M. Winfield, D. Lennon, Phys. Chem. Chem. Phys. 7 (2005) 565.
[27] S. Bertarione, D. Scarano, A. Zecchina, V. Johanek, J. Hoffmann, S. Schauermann, M.M. Frank, J. Libuda, G. Rupprechter, H.-J. Freund, J. Phys. Chem. B 108 (2004) 3603.
[28] S. Bertarione, D. Scarano, A. Zecchina, V. Johanek, J. Hoffmann, S. Schauermann, J. Libuda, G. Rupprechter, H.-J. Freund, J. Catal. 223 (2004) 64.
[29] S. Giorgio, C. Chapon, C.R. Henry, Langmuir 13 (1997) 2279.
[30] M. Sterrer, T. Risse, H.-J. Freund, Surf. Sci. 596 (2005) 222.
[31] M.A. Babaeva, D.S. Bystrov, A.Yu. Kovalgin, A.A. Tsyganenko, J. Catal. 123 (1990) 396.
[32] D.G. Rethwisch, J.A. Dumesic, Langmuir 2 (1986) 73.
[33] K. Teramura, T. Tanaka, H. Ishikawa, Y. Kohno, T. Funabiki, J. Phys. Chem. B 108 (2004) 346.
[34] A.A. Davydov, Infrared Spectroscopy of Adsorbed Species on the Surface of Transition Metal Oxides, Wiley, Chichester, 1990.
[35] K.I. Hadjiivanov, G.N. Vayssilov, Adv. Catal. 47 (2002) 307.
[36] M. Bailes, F.S. Stone, Mater. Chem. Phys. 29 (1991) 489.
[37] R.St.C. Smart, T.L. Slager, L.H. Little, R.G. Greenler, J. Phys. Chem. 77 (1973) 1019.
[38] Y. Yanagisawa, K. Takaoka, S. Yamabe, T. Ito, J. Phys. Chem. 99 (1995) 3704.
[39] X.D. Peng, M.A. Barteau, Surf. Sci. 233 (1990) 283.
[40] C. Goyhenex, M. Croci, C. Claeys, C.R. Henry, Surf. Sci. 352–354 (1996) 475.
[41] K. Wolter, O. Seiferth, H. Kuhlenbeck, M. Bäumer, H.-J. Freund, Surf. Sci. 399 (1998) 190.
[42] M. Bäumer, H.-J. Freund, Prog. Surf. Sci. 61 (1999) 127.
[43] I.V. Yudanov, R. Sahnoun, K.M. Neyman, N. Rösch, J. Hoffmann, S. Schauermann, V. Johánek, H. Unterhalt, G. Rupprechter, J. Libuda, H.-J. Freund, J. Phys. Chem. B 107 (2003) 255.
[44] G. Rupprechter, H. Unterhalt, M. Morkel, P. Galletto, L. Hu, H.-J. Freund, Surf. Sci. 502–503 (2002) 109.
[45] M. Morkel, H. Unterhalt, M. Salmeron, G. Rupprechter, H.-J. Freund, Surf. Sci. 532–535 (2003) 103.
[46] B. Hammer, J.K. Norskov, in: R.M. Lambert, G. Pacchioni (Eds.), Chemisorption and Reactivity on Supported Clusters and Thin Films, in: NATO ASI Series E, Kluwer, Dordrecht, 1997.
[47] R. van Hardeveld, F. Hartog, Surf. Sci. 15 (1969) 189.
[48] A. Wille, P. Nickut, K. Al-Shamery, J. Mol. Struct. 695–696 (2004) 345.
[49] V.G. Kulebakin, V.N. Koptelov, L.D. Bocharov, Yu.A. Dmitrienko, P.S. Polovinkina, Refract. Ind. Ceram. 34 (1993) 148.
[50] Sh.K. Shaikhutdinov, M. Frank, M. Bäumer, S.D. Jackson, R.J. Oldman, J.C. Hemminger, H.-J. Freund, Catal. Lett. 80 (2002) 115.
[51] M. Morkel, V.V. Kaichev, G. Rupprechter, H.-J. Freund, I.P. Prosvirin, V.I. Bukhtiyarov, J. Phys. Chem. B 108 (2004) 12955.
[52] A. Ludviksson, R. Zhang, C.T. Campbell, K. Griffiths, Surf. Sci. 313 (1994) 64.
[53] O. Demoulin, G. Rupprechter, I. Seunier, B. Le Clef, M. Navez, P. Ruiz, J. Phys. Chem. B 109 (2005) 20454.
[54] T. Schalow, B. Brandt, M. Laurin, S. Schauermann, J. Libuda, H.-J. Freund, J. Catal. 242 (2006) 58.
[55] H. Gabasch, A. Knop-Gericke, R. Schlögl, M. Borasio, C. Weilach, G. Rupprechter, S. Penner, B. Jenewein, K. Hayek, B. Klötzer, Phys. Chem. Chem. Phys. 9 (2007) 533.
[56] T. Schalow, B. Brandt, D.E. Starr, M. Laurin, S. Schauermann, S.K. Shaikhutdinov, J. Libuda, H.-J. Freund, Catal. Lett. 107 (2006) 189.
[57] H. Gabasch, W. Unterberger, K. Hayek, B. Klötzer, E. Kleimenov, D. Teschner, S. Zafeiratos, M. Hävecker, A. Knop-Gericke, R. Schlögl, J. Han, F.H. Ribeiro, B. Aszalos-Kiss, T. Curtin, D. Zemlyanov, Surf. Sci. 600 (2006) 2980.
[58] T. Engel, G. Ertl, in: D.A. King, D.P. Woodruff (Eds.), The Chemical Physics of Solid Surfaces and Heterogeneous Catalysis, vol. 4, Elsevier, Amsterdam, 1982, p. 73.
[59] G. Rupprechter, M. Morkel, H.-J. Freund, R. Hirschl, Surf. Sci. 554 (2004) 43.
[60] M. Morkel, G. Rupprechter, H.-J. Freund, Surf. Sci. Lett. 588 (2005) L209.